







Optical Polarimetry of the Tidal Disruption Event AT2019DSG

Chien-Hsiu Lee (李見修)¹ , Tiara Hung², Thomas Matheson¹ , Monika Soraisam^{3,4}, Gautham Narayan⁴ , Abhijita Saha¹ ,
Carl Stubens¹, and Nicholas Wolf¹

¹ NSF's National Optical-Infrared Astronomy Research Laboratory, Tucson, AZ, USA; lee@noao.edu

² University of California, Santa Cruz, CA, USA

³ National Center for Supercomputing Applications, Urbana, IL, USA

⁴ University of Illinois at Urbana-Champaign, Urbana, IL, USA

Received 2019 August 14; revised 2020 February 29; accepted 2020 March 5; published 2020 March 18

Abstract

We present time-series imaging polarimetry observations of a nearby tidal disruption event (TDE) AT2019DSG at $z = 0.0512$ to probe the disruption mechanism and shed light on the accretion process. We obtain linear polarimetry using the Alhambra Faint Object Spectrograph and Camera on board the 2.5 m Nordic Optical Telescope. Our observations showed a polarization at the $9.2\% \pm 2.7\%$ level early on, decreasing to less than 2.7% (at the 68% confidence level) one month later. While the high level of polarization in the early epoch is similar to that of Swift J164449.3+573451 and Swift J2058+0516, the low level of polarization in the later epoch is in agreement with that of OGLE16aaa. Our results thus show the temporal evolution of optical polarization from a TDE. As the degree of polarization changes over time, it is unlikely to be attributed to host galaxy dust, but may originate from a non-isotropic accreting disk, or associated with the relativistic jet emission.

Unified Astronomy Thesaurus concepts: Tidal disruption (1696); Polarimetry (1278)

1. Introduction

Tidal disruption events (TDEs) are flaring phenomena when a stellar object passes close to the super massive black hole (SMBH) in the center of a galaxy. The stellar object is torn apart by the tidal force of the SMBH and generates a flare when accreted onto the SMBH. In this regard, TDEs are excellent probes of the SMBHs during quiescence, e.g., the mass and spin of the black holes (Mockler et al. 2019), which are otherwise hard to detect and characterize. In addition, accompanied by the TDE there may be relativistic jets launched by the accretion on to the SMBH (Curd & Narayan 2019), hence providing insight into the accretion mechanism of AGNs. In this regard, polarimetry observations are especially useful to probe the jet formation physics and the geometry of the accretion disk around the SMBH revealed by TDE events. However, as the event rate of TDE is relative low, $\sim 10^{-5}$ per galaxy per year (Holoien et al. 2016), there were only a few imaging linear polarimetric measurements of a handful of TDEs at very late stage, e.g., Swift J164449.3+573451 (Wiersema et al. 2012), OGLE16aaa (Higgins et al. 2019), and Swift J2058+0516 (Wiersema et al. 2020). The degrees of polarization of these TDE events varied significantly; Wiersema et al. (2012) showed a polarization of 7.4%, while Higgins et al. (2019) found a relatively low degree of polarization at 1.8%. This might be because the former had a bright relativistic jet, whereas the later was a thermal TDE. In addition, Wiersema et al. (2020) recently reported the time-varied polarization of Swift J2058+0516, which could originate from nonthermal emission from the relativistic jet. As there are only a few polarimetric observations of only three TDEs, performing polarimetric observations of a larger number of TDEs, with and without relativistic jets, is important to understand the polarimetric properties and shed light on the TDE formation mechanisms.

The vast majority of TDEs are relatively faint (see, e.g., the Open Tidal Disruption Event catalog⁵), resulting in low signal-to-

noise ratio (S/N) even in imaging polarimetry, thus hampering high-precision measurements of polarization. However, all-sky surveys like the All-Sky Automated Survey for Supernovae (ASAS-SN; Shappee et al. 2014) and Zwicky Transient Facility (ZTF; Bellm et al. 2019) have changed this situation by providing bright TDEs in nearby galaxies. Here we present timely cadenced imaging polarimetry of AT2019DSG, a bright TDE ($R = 17.9$ mag) recently confirmed in 2019 May by ePESSTO+ collaboration (Nicholl et al. 2019). It is very close to the center of its host (at a separation of $0''.1$ from ZTF astrometry), passing the $<0''.6$ separation criterion of selecting ZTF TDE events by van Velzen et al. (2019). The proximity of the host galaxy (at a redshift of $z = 0.05$), bright nature of AT2019DSG, and the fact that it was discovered before passing the peak brightness make AT2019DSG a promising TDE target for imaging polarimetry observations.

This Letter is organized as follows. In Section 2 we describe our Alhambra Faint Object Spectrograph and Camera (ALFOSC) polarimetry observations. In Section 3 we present results from polarimetry analysis, to derive the degree of polarization at different epochs; we also compare our results to other studies, followed by a summary in Section 4.

2. Observation

AT2019DSG was first reported by the ZTF survey as ZTF19aapreis on 2019 April 9, with 18.88 mag in the r filter (Nordin et al. 2019). The The Asteroid Terrestrial-impact Last Alert System (ATLAS; Tonry et al. 2018) team also picked up this transient as ATLAS19klx on 2019 May 12, with 17.993 mag in the orange-ATLAS filter (Tonry et al. 2019). Both ZTF and ATLAS provided a preliminary classification of AT2019DSG as a possible supernova. Spectroscopic follow-up on 2019 May 13, by the advanced extended Public ESO Spectroscopic Survey for Transient Objects (ePESSTO+) showed that AT2019DSG is actually a tidal disruption event rather than a supernova explosion (Nicholl et al. 2019). The ePESSTO+ team also determined

⁵ <https://tde.space/>

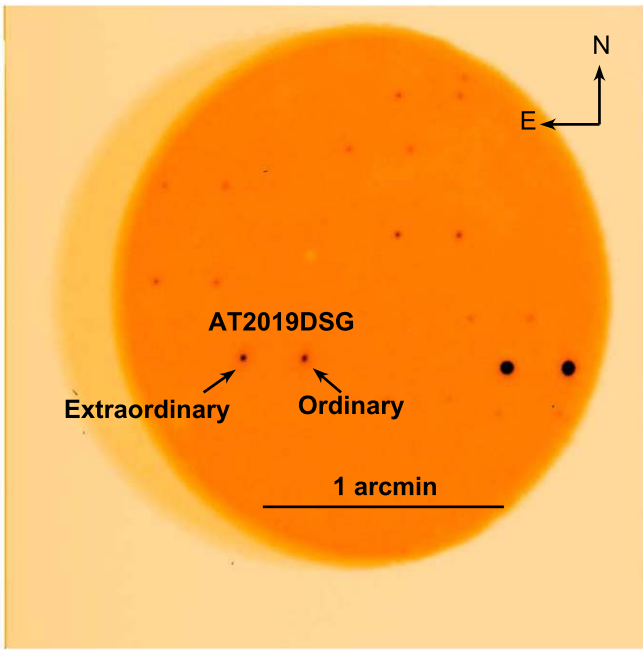


Figure 1. Imaging polarimetry of AT2019DSG by ALFOSC in the V band with a 200 s exposure time on 2019 June 20. We acquired imaging polarimetry through half-wave plate angles of 0° , 22.5° , 45° , and 67.5° . The half-wave plate split the light from the TDE into ordinary and extraordinary beams, separated by $\sim 15''$ as indicated by the arrows. We also used the bright field star, $\sim 1'$ west to AT2019DSG, to evaluate line-of-sight polarization.

the redshift of AT2019DSG to be $z = 0.0512$ based on the host galaxy. AT2019DSG was relatively bright and on the rise to the peak on May 13, as shown by the ZTF public-survey light curves from the ANTARES alert-broker⁶ (Saha et al. 2014, 2016; Narayan et al. 2018) in Figure 3. It reached its peak brightness of 18 mag (both in the g and R bands) in mid-May. We thus requested fast-track service observations at the Nordic Optical Telescope using its ALFOSC in the linear imaging polarimetry mode to monitor the change in polarization during the course of brightening and fading of AT2019DSG. The polarimetry mode of ALFOSC split the source light into two orthogonally polarized beams, i.e., ordinary and extraordinary components, on the same image separated by $\sim 15''$ (see Figure 1). Observations were conducted in the V band at four different half-wave plate angles (0° , 22.5° , 45° , and 67.5°). Given the bright nature of AT2019DSG reported by ATLAS on 2019 May 12, a few minutes of integration time per half-wave plate angle would be able to deliver relatively high polarization precision, enabling us to detect the polarization signal to study the accretion process of the TDEs (see, e.g., Wiersema et al. 2020). We thus obtained two epochs of polarimetry observations, on 2019 May 17 and June 20, respectively, to study the temporal evolution of the degree of polarization. In addition to our target, we also observed a high polarization standard Hiltner 960 and a zero polarization standard BD+28 4211, which were chosen because they are close to the target on the sky with a similar R.A. Both standard stars were observed along with the target on both of the nights of May 17 and June 20, respectively. The observation log can be found in Table 1.

⁶ <https://antares.noao.edu>

Table 1
Observation Log

UT Date	Target	Exp. Time	Seeing
Epoch 1			
2019 May 17 04:19–04:20	High polarization standard	4×1 s	1.5
2019 May 17 04:26–04:32	AT2019DSG	4×100 s	1.5
2019 May 17 04:39–04:40	Zero polarization standard	4×1 s	1.5
Epoch 2			
2019 Jun 20 03:28–03:39	AT2019DSG	4×200 s	0.8
2019 Jun 20 03:48–03:49	High polarization standard	4×1 s	0.8
2019 Jun 20 03:52–03:53	Zero polarization standard	4×1 s	0.8

3. Data Analysis and Results

The data reduction was carried out in a standard manner using IRAF.⁷ The polarimetry images were first bias-subtracted and flat-fielded. After de-trending, we then proceeded to obtain the flux of the ordinary and extraordinary components. Please note that after the half-wave plate, the polarized images of AT2019DSG were not circular, hence making point-spread function (PSF) photometry difficult. To surmount this issue, we used aperture photometry instead of PSF fitting, to better extract the photometry. We used a fixed aperture size of two times the size of the FWHM of the point-spread function, and extracted the photometry using SExtractor (Bertin & Arnouts 1996). With the flux of ordinary and extraordinary beams in hand, we can proceed to derive the linear polarization, following Patat & Romaniello (2006), who introduced the normalized flux differences F_i as

$$F_i = \frac{f_{O,i} - f_{E,i}}{f_{O,i} + f_{E,i}}, \quad (1)$$

where $f_{O,i}$ and $f_{E,i}$ are flux from ordinary and extraordinary beams from the i th half-wave plate angle. With the normalized flux differences, we can thus derive the normalized Stokes parameters \bar{Q} and \bar{U} :

$$\bar{Q} = \frac{Q}{I} = \frac{1}{2} \sum_{i=0}^3 F_i \cos\left(\frac{\pi i}{2}\right), \quad (2)$$

$$\bar{U} = \frac{U}{I} = \frac{1}{2} \sum_{i=0}^3 F_i \sin\left(\frac{\pi i}{2}\right), \quad (3)$$

where I is the Stokes parameter for polarization intensity and Q and U describe the linear polarization (see, e.g., Chandrasekhar 1950). The degree of linear polarization P is then

$$P = \frac{\sqrt{Q^2 + U^2}}{I} = \sqrt{\bar{Q}^2 + \bar{U}^2}. \quad (4)$$

With these formulae, we derived a polarization of $9.6\% \pm 2.6\%$ and $2.0\% \pm 1.0\%$ on 2019 May 17 and June 20, respectively for our observations of AT2019DSG. In addition, we also obtained polarimetry of strongly polarized

⁷ <http://iraf.noao.edu/>

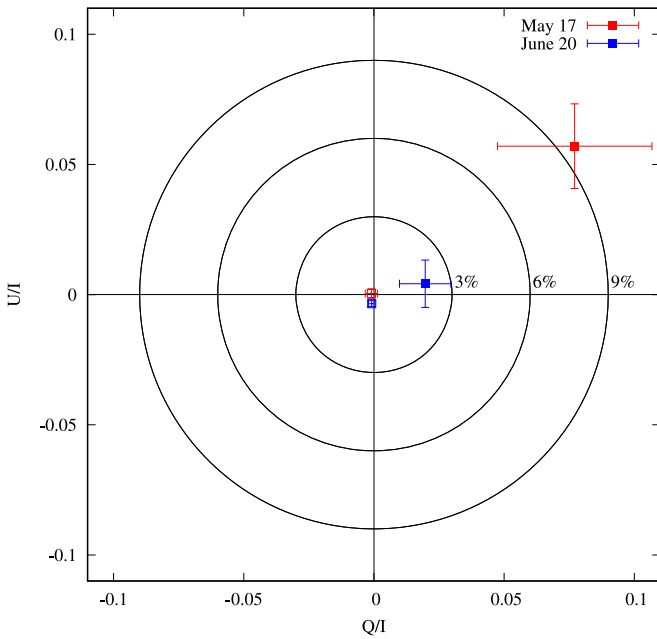


Figure 2. Polarization measurement at two epochs of AT2019DSG on 2019 May 17 (red filled square) and June 20 (blue filled square). The x - and y -axes are normalized Stokes parameter \bar{Q} and \bar{U} , respectively. The two epochs show different level of polarization, indicating the degree of polarization decreases over time. We also plot the polarization measurements of the field star in red and blue open squares, corresponding to 2019 May 17 and June 20, respectively.

standard star Hiltner 960 and zero polarization standard star BD +28_4211, which all showed degrees of polarization consistent with literature values. The polarization measurements of \bar{Q} and \bar{U} are shown in Figure 2 and Table 2.

In order to correct for polarization bias, we use the modified asymptotic (MAS) estimator by Plaszczyński et al. (2014):

$$P_{\text{MAS}} = P - \sigma^2 \frac{1 - e^{-\frac{P^2}{\sigma^2}}}{2P}, \quad (5)$$

where P_{MAS} is the estimation of true polarization, and the variance of P can be determined as

$$\sigma = \sqrt{\frac{\bar{Q}^2 \sigma_{\bar{Q}}^2 + \bar{U}^2 \sigma_{\bar{U}}^2}{\bar{Q}^2 + \bar{U}^2}}, \quad (6)$$

where $\sigma_{\bar{Q}}$ and $\sigma_{\bar{U}}$ correspond to the standard error of \bar{Q} and \bar{U} . We thus use the respective \bar{Q} and \bar{U} of AT2019DSG, and take into account both the standard error and statistical error (0.05% in \bar{Q} and 0.1% in \bar{U} from the highly polarized standard star) to calculate P_{MAS} . For the first epoch of AT2019DSG, we obtained $P_{\text{MAS}} = 9.2\%$ and $\sigma = 2.7\%$, with $P_{\text{MAS}}/\sigma > 3$.

For our second epoch of AT2019DSG, the S/N is too low (< 3), hence the polarization no longer follows a Gaussian distribution, but a Rice distribution instead (Plaszczyński et al. 2014). To obtain a robust estimate of the upper limit, we used the formulation by Plaszczyński et al. (2014). More specifically, for a 68% confidence level (corresponding to 1σ), the upper limit can be estimated as:

$$P_{\text{upper}}^{68\%} = P_{\text{MAS}} + (1 - 0.97 \times e^{-2.01 \times P_{\text{MAS}}}). \quad (7)$$

We thus obtained an upper limit of 2.7% at the 1σ level for the second epoch of AT2019DSG.

Table 2
Polarization Measurements

Target	\bar{Q} (%)	\bar{U} (%)	P (%)	θ ($^\circ$)
Epoch 1—2019 May 17				
AT2019DSG	7.7 ± 3.0	5.7 ± 1.6	9.6 ± 2.6	18.2 ± 0.2
Zero polarization standard	0.2 ± 0.1	0.1 ± 0.1	0.2 ± 0.1	...
High polarization standard	-2.0 ± 0.1	5.2 ± 0.1	5.6 ± 0.1	55.7 ± 0.1
Field Star	-0.1 ± 0.2	0.0 ± 0.2	0.1 ± 0.2	...
Epoch 2—2019 June 20				
AT2019DSG	2.0 ± 1.0	0.4 ± 1.0	2.0 ± 1.0	6.0 ± 0.5
Zero polarization standard	-0.1 ± 0.1	-0.1 ± 0.1	0.2 ± 0.1	...
High polarization standard	-1.9 ± 0.1	5.0 ± 0.1	5.4 ± 0.1	55.4 ± 0.1
Field Star	-0.1 ± 0.1	-0.3 ± 0.1	0.4 ± 0.1	...

It appears that AT2019DSG exhibits a polarization of $\sim 2\%$ at the later epoch. However, we also need to take into account the interstellar polarization (ISP), which comes from the line-of-sight dust contributed by the Milky Way (MWG) and the host galaxy. By checking the extinction map, the line-of-sight MWG extinction— $E(B-V)$ —is ~ 0.088 from Schlafly & Finkbeiner (2011) and 0.102 from Schlegel et al. (1998). According to the empirical upper limits from Serkowski et al. (1975), this can translate into P as high as $\sim 1\%$. Another way to measure line-of-sight MWG dust polarization is to use field stars. In this regard, we also measure the polarization of a bright field star $\sim 1'$ west of AT2019DSG. The field star polarization is at $< 0.5\%$ level, consistent with the empirical upper limits from Serkowski et al. (1975). In addition to line-of-sight MWG dust polarization, there can also be polarization coming from the host. To constrain it, we used multiband photometry from Pan-STARRS (Chambers et al. 2016) and fit the host galaxy spectral energy distribution (SED) with LePhare (Arnouts et al. 1999; Ilbert et al. 2006). This gives an $E(B-V)$ of 0.05, relatively small compared to the line-of-sight MWG extinction, hence the host galaxy plays an insignificant role in contributing to the polarization. This suggests that the high polarization ($\sim 9\%$) in the optical in the earlier epoch cannot be explained by the MWG dust extinction alone. This is different from the case of Swift J164449.3+573451, where there was no polarization in the radio wavelength, and Wiersema et al. (2012) attributed the high linear polarization in the near-infrared to the dust induced polarization by the host galaxy.

We also include a light curve of AT2019DSG from the alerts issued by the public ZTF survey, aggregated by the community broker ANTARES⁸ (Saha et al. 2014, 2016; Narayan et al. 2018) in both g and r bands, as shown in Figure 3. With the light curve in hand, we can also check whether the TDE faded significantly between the first and second epoch, and whether the polarization signal is diluted (hence reduced) by the light from host galaxy. As can be seen in Figure 3, the light curve indicates that the brightness of the TDE decreased from 17.87 ± 0.06 mag to 18.46 ± 0.10 mag in the g band between the two epochs. We note that the ZTF

⁸ <https://antares.noao.edu>

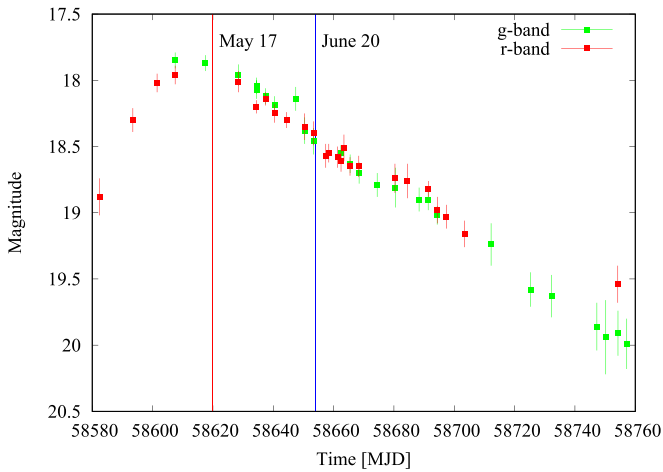


Figure 3. The *g*- and *r*-band light curve of AT2019DSG. The data points are from the public ZTF survey alerts that are associated with AT2019DSG, and aggregated by the community broker ANTARES. The timing of the two polarization observation epochs of AT2019DSG on 2019 May 17 and June 20 are also marked, respectively. The full AT2019DSG light curve from ANTARES can be accessed at <https://antares.noao.edu/alerts/locus/2878127>.

measurement is based on difference imaging, meaning that the photometry is solely from the light of TDE, excluding the host galaxy. In comparison, the host galaxy has a magnitude of 18.33 mag in the ZTF reference image. If the intrinsic TDE polarization were constant, then the observed decrease in the TDE flux (when combined with that from host galaxy) would imply a 25% drop in the polarization, down to the $\sim 7\%$ level. However, since we observed the polarization decreased drastically to the 2% level, it indicates that the intrinsic TDE polarization is dropping rapidly between two epochs.

We note that TDEs can be generally categorized into thermal (i.e., with a blackbody optical SED) and relativistic (i.e., exhibiting a strong radio counterpart indicating the launch of a bright relativistic jet). Currently there are only a few relativistic TDEs known, e.g., Swift J1644+57 (Bloom et al. 2011), Swift J2058+0516 (Cenko et al. 2012), Swift J1112.2-8238 (Brown et al. 2015), ASASSN-14li (Alexander et al. 2016), Arp299B-AT1 (Mattila et al. 2018), and AT2019azh (Perez-Torres et al. 2019), while there are many thermal TDEs with deep limits in the radio that rule out jet activities. While it is likely that these two classes are closely related—for example, Swift J2058+0516 has a thermal optical spectrum and also a strong jet—it is important to distinguish these two classes as relativistic TDEs exhibit nonthermal (e.g., synchrotron) emission in the radio and will have a tail into the optical, leading to detectable polarization. Given the unambiguous detection in the radio, AT2019DSG thus belongs to the class of relativistic TDEs (Perez-Torres et al. 2019). We should note that the radio detection is not at the exactly same time as X-ray observations or our optical imaging polarimetric observations, and with only one radio band, it is difficult to compare to or obtain a meaningful SED. Simultaneous multiwavelength observations for future TDE events will be greatly helpful to provide insightful tests for modeling. Nevertheless, we provide a qualitative discussion on the origins of polarization of AT2019DSG as follows.

From the multiwavelength data of Swift J164449.3+573451, Bloom et al. (2011) interpreted the SED with two components: the peak at the radio wavelength is consistent with synchrotron

radiation, and the other peak at the X-ray wavelength is consistent with inverse self-Compton. This suggests that the TDE is powered by forward shock, similar to the afterglow of gamma-ray bursts (GRBs). In a similar system (Swift J2058.4+0516), Pasham et al. (2015) also reached the same conclusion that the SED is best explained by a forward shock. In that case, unless the shocked accretion disk was non-isotropic, it is expected that the optical polarization will be at a very low degree. Hence, our detection of high polarization in the optical may suggest that the accretion disk is rather non-isotropic. Indeed, Liu et al. (2017) have proposed a model of an elliptical (instead of circularized) accretion disk that can explain the complex and diverse profiles seen in the optical/UV discovered TDE PTF09dj1. However, the vanishing polarization from our observations would imply that the accretion disk changes from elliptical to circular in a month, which is unlikely. In addition to the non-isotropic accretion disk, theoretical studies of GRB afterglows (see, e.g., Gill et al. 2020) demonstrated that late-time GRB afterglows can show linear polarization values as high as 5%, and a value of 10% is not unlikely if the jet is structured or seen at a large off-axis angle. Indeed, recent studies of Swift J2058 by Wiersema et al. (2020) reported a polarization value of $\sim 8\%$ in the optical (similar to the optical polarization value reported in this work), and attributed the linear polarization to TDE jet emission.

On the other hand, it has been shown that blazars can exhibit varying polarization (Krawczynski 2012), which originates from the backward shock instead of the forward shock. However, X-ray observations (contemporary to our optical polarimetry) by Swift (Pasham et al. 2019b) and NICER (Pasham et al. 2019a) can be well fitted with a simple accretion disk without introducing a Comptonized term, hence the polarization is unlikely to be triggered as seen in the blazars.

4. Summary

We present imaging polarimetry results of the recently discovered nearby tidal disruption event AT2019DSG. Our studies can be summarized as follows:

1. Using ALFOSC, we obtained two epochs of imaging polarimetry. The early epoch shows a significant amount of polarization in the optical, but dropping rapidly in the later epoch, suggesting a vanishing polarization.
2. Using the extinction map, we obtain a line-of-sight $E(B-V) \sim 0.1$. This translates to a $< 1\%$ polarization from dust in the MWG. Even if we attributed the rest of the polarization in the later epoch to the host galaxy, it is only a small fraction of the high polarization seen in the early epoch. This suggests that there is a significant amount of polarization detected in the optical in the earlier epoch from the tidal disruption event itself.
3. The high degree of polarization in the optical is inconsistent with the forward-shock model of the isotropic accretion disk. While it is plausible a non-isotropic accretion can accommodate the high degree of polarization at the first epoch, it is inconsistent with the vanishing polarization at the later epoch. Thus, it is likely that there is nonnegligible contribution from the relativistic jet emission to the optical flux of AT2019DSG.

We are indebted to the anonymous referee, whose comments greatly improved the manuscript. We are grateful to the staff at

the Nordic Optical Telescope for scheduling and carrying out timely and flexible observations under the fast-track service program. This work is based on observations made with the Nordic Optical Telescope, operated by the Nordic Optical Telescope Scientific Association at the Observatorio del Roque de los Muchachos, La Palma, Spain, of the Instituto de Astrofísica de Canarias. The data presented here were obtained with ALFOSC, which is provided by the Instituto de Astrofísica de Andalucía (IAA) under a joint agreement with the University of Copenhagen and NOTSA.

ORCID iDs

Chien-Hsiu Lee (李見修)  <https://orcid.org/0000-0003-1700-5740>

Thomas Matheson  <https://orcid.org/0000-0001-6685-0479>

Gautham Narayan  <https://orcid.org/0000-0001-6022-0484>

Abhjita Saha  <https://orcid.org/0000-0002-6839-4881>

References

- Alexander, K. D., Berger, E., Guillochon, J., et al. 2016, *ApJL*, 819, L25
- Arnouts, S., Cristiani, S., Moscardini, L., et al. 1999, *MNRAS*, 310, 540
- Bellm, E. C., Kulkarni, S. R., Graham, M. J., et al. 2019, *PASP*, 131, 018002
- Bertin, E., & Arnouts, S. 1996, *A&AS*, 117, 393
- Bloom, J. S., Giannios, D., Metzger, B. D., et al. 2011, *Sci*, 333, 203
- Brown, G. C., Levan, A. J., Stanway, E. R., et al. 2015, *MNRAS*, 452, 4297
- Cenko, S. B., Krimm, H. A., Horesh, A., et al. 2012, *ApJ*, 753, 77
- Chambers, K. C., Magnier, E. A., Metcalfe, N., et al. 2016, arXiv:1612.05560
- Chandrasekhar, S. 1950, *Radiative Transfer* (Oxford: Clarendon Press)
- Curd, B., & Narayan, R. 2019, *MNRAS*, 483, 565
- Gill, R., Granot, J., & Kumar, P. 2020, *MNRAS*, 491, 3343
- Higgins, A. B., Wiersema, K., Covino, S., et al. 2019, *MNRAS*, 482, 5023
- Holoien, T. W.-S., Kochanek, C. S., Prieto, J. L., et al. 2016, *MNRAS*, 455, 2918
- Ilbert, O., Arnouts, S., McCracken, H. J., et al. 2006, *A&A*, 457, 841
- Krawczynski, H. 2012, *ApJ*, 744, 30
- Liu, F. K., Zhou, Z. Q., Cao, R., et al. 2017, *MNRAS*, 472, L99
- Mattila, S., Pérez-Torres, M., Efstathiou, A., et al. 2018, *Sci*, 361, 482
- Mockler, B., Guillochon, J., & Ramirez-Ruiz, E. 2019, *ApJ*, 872, 151
- Narayan, G., Zaidi, T., Soraisam, M. D., et al. 2018, *ApJS*, 236, 9
- Nicholl, M., Short, P., Angus, C., et al. 2019, *ATel*, 12752, 1
- Nordin, J., Brinnet, V., Giomi, M., et al. 2019, *TNSTR*, 615, 1
- Pasham, D., Remillard, R., Loewenstein, M., et al. 2019a, *ATel*, 12825, 1
- Pasham, D., Remillard, R., & Wevers, T. 2019b, *ATel*, 12777, 1
- Pasham, D. R., Cenko, S. B., Levan, A. J., et al. 2015, *ApJ*, 805, 68
- Patat, F., & Romaniello, M. 2006, *PASP*, 118, 146
- Perez-Torres, M., Moldon, J., Mattila, S., et al. 2019, *ATel*, 12870, 1
- Perez-Torres, M., Moldon, J., Mattila, S., et al. 2019, *ATel*, 12960, 1
- Plaszczynski, S., Montier, L., Levrier, F., et al. 2014, *MNRAS*, 439, 4048
- Saha, A., Matheson, T., Snodgrass, R., et al. 2014, *Proc. SPIE*, 9149, 914908
- Saha, A., Wang, Z., Matheson, T., et al. 2016, *Proc. SPIE*, 9910, 99100F
- Schlafly, E. F., & Finkbeiner, D. P. 2011, *ApJ*, 737, 103
- Schlegel, D. J., Finkbeiner, D. P., & Davis, M. 1998, *ApJ*, 500, 525
- Serkowski, K., Mathewson, D. S., & Ford, V. L. 1975, *ApJ*, 196, 261
- Shappee, B. J., Prieto, J. L., Grupe, D., et al. 2014, *ApJ*, 788, 48
- Tonry, J., Denneau, L., Heinze, A., et al. 2019, *TNSTR*, 758, 1
- Tonry, J. L., Denneau, L., Heinze, A. N., et al. 2018, *PASP*, 130, 064505
- van Velzen, S., Gezari, S., Cenko, S. B., et al. 2019, *ApJ*, 872, 198
- Wiersema, K., Higgins, A. B., Levan, A. J., et al. 2020, *MNRAS*, 491, 1771
- Wiersema, K., van der Horst, A. J., Levan, A. J., et al. 2012, *MNRAS*, 421, 1942